International Journal of Computational and Experimental Science and ENgineering (IJCESEN)

Vol.10 -No.4 (2024) pp.592-613
http://www.ijcesen.com

ISSN: 2149-9144

Research Article

A novel lightweight deep learning model based on SqueezeNet architecture for viral lung disease classification in X-ray and CT images

Abhishek AGNIHOTRI[1]*, Narendra KOHLI[2]

[1] Computer Science and Engineering Department, Harcourt Butler Technical University, 208002, Kanpur, India
* **Corresponding Author Email:** abhiagni1991@gmail.com **ORCID:** 0000-0001-5213-0382

[2] Computer Science and Engineering Department, Harcourt Butler Technical University, 208002, Kanpur, India
Email: nkohli@hbtu.ac.in **ORCID:** 0000-0002-9407-3598

Article Info:

DOI: 10.22399/ijcesen.425
Received: 22 August 2024
Accepted: 25 September 2024

Keywords

Lightweight
ECA
Attention Mechanism
Pneumonia
Covid-19

Abstract:

COVID-19 has affected hundreds of millions of individuals, seriously harming the global population's health, welfare, and economy. Furthermore, health facilities are severely overburdened due to the record number of COVID-19 cases, which makes prompt and accurate diagnosis difficult. Automatically identifying infected individuals and promptly placing them under special care is a critical step in reducing the burden of such issues. Convolutional Neural Networks (CNN) and other machine learning techniques can be utilized to address this demand. Many existing Deep learning models, albeit producing the intended outcomes, were developed using millions of parameters, making them unsuitable for use on devices with constrained resources. Motivated by this fact, a novel lightweight deep learning model based on Efficient Channel Attention (ECA) module and SqueezeNet architecture, is developed in this work to identify COVID-19 patients from chest X-ray and CT images in the initial phases of the disease. After the proposed lightweight model was tested on different datasets with two, three and four classes, the results show its better performance over existing models. The outcomes shown that, in comparison to the current heavyweight models, our models reduced the cost and memory requirements for computing resources dramatically, while still achieving comparable performance. These results support the notion that proposed model can help diagnose Covid-19 in patients by being easily implemented on low-resource and low-processing devices.

1. Introduction

COVID-19 infection is caused by SARS-CoV-2. COVID-19 virus causes holes in lungs that resemble honeycombs [1]. The Covid-19 pandemic response on a worldwide scale has brought attention to the connection between public health and lung health, underscoring the need for further research and collaboration in the realm of lung infections. Total 53,883 cases are reported by WHO (data as of 7 days to July 28, 2024, https://data.who.int/dashboards/covid19/cases).
Several Covid-19 fatalities had severe chest congestion, which led to a significant drop in oxygen levels and an increased risk of major heart attacks [2]. Moreover, inflammation in the lungs' tiny air sacs is a feature of pneumonia, another form of lung illness. Numerous infections, such as bacteria, viruses, or fungus, may be the cause [3]. It is interesting to note that Covid-19 and pneumonia share comparable indications and symptoms [4]. It becomes essential to correctly identify diseases because of this strong relationship and the fact that various diseases require different treatment [5]. This guarantees that several treatment techniques, tailored to the lung disease, can be used. This study attempts to determine the classes as pneumonia, Covid-19, lung opacity, and healthy as a result.
Reverse transcription polymerase chain reaction is currently the standard method for Covid-19 screening [6]. Nevertheless, this test kit takes a while to complete (results usually show up in a few hours or days). In addition, it is not generally accessible, especially in underdeveloped nations, and only possesses a 63.0% sensitivity rate [7,8]. To detect individuals with Covid-19 and save many lives, various diagnostic techniques must be taken into consideration. Thankfully, it has been discovered

that imaging techniques for chest radiography are useful in this regard. This is because abnormalities in chest radiography images, which aid in distinguishing between healthy and infected subjects, may be identified. Covid-19 mostly affects the lungs [9].

In clinical practice, Chest X-rays (CXR), and computed tomography (CT) are currently the two imaging modalities used to assess and diagnose Covid-19 [10,11]. CXRs are utilized in medical facilities more frequently than CT scans because of their low radiation dose, affordability, convenience of use, and general accessibility. Despite using CXRs frequently in Covid-19 diagnosis, many Artificial intelligence (AI)-based diagnosis systems are developing to combat the Covid-19 using CT scans in its early stage [12]. To distinguish Covid-19 instances from others, many CXR images must be manually analysed, which take time and effort [13,14]. Moreover, it might be difficult, even for experienced radiologists, to interpret CXRs images for Covid-19 diagnosis. On CXRs, Covid-19 frequently seems vague and might mimic the symptoms of other lung ailments or be misdiagnosed as other lung diseases [15]. Computer aided diagnostic technologies are needed to help radiologists diagnose Covid-19 from CXRs. Particularly in its subfield of machine learning (ML) [16] and deep learning (DL) [17,18], AI has demonstrated greater success in computer vision tasks. These advances have been applied in a range of disciplines recently to support medical professionals in early diagnosis of diseases like brain tumour detection, stress [19,20], anxiety [21], sleep disorders [22,23], diabetes retinopathy, and lung disease prediction [4]. Because of their effectiveness, these CXR image-based models can identify COVID-19 cases. Covid-19 diagnosis from CXRs remains challenging, but to improve early diagnosis and lower the annual mortality rate, highly reliable and effective automated diagnostic procedures for Covid-19 identification must be developed [24]. Yasar et al., 2024 [67] proposed twenty-four layered CNN model for binary classification of Covid-19 with CT images. Their proposed approach was achieved 95.77% accuracy. Hassan et al., 2024 [68] proposed the DCNN model based on transfer learning. They analysed InceptionV3, VGG-16, VGG-19, and Resnet50 as feature extractor in proposed DCNN model. Their proposed approach got an 99.07% accuracy with ResNet50 as feature extractor and ADAM optimizer. Zhang et al., 2024 [69] proposed the CNN model with attention mechanism called Cn2a-capsnet. They performed the experiment on CXR images, and got an accuracy of 98.54% and 96.71% accuracy in binary and multiclass classification respectively.

In numerous applications, including computer vision, robotic control, and speech recognition, deep neural networks (DNNs) [25] have demonstrated remarkable success. DNNs extract features from datasets and achieve remarkable performances in a variety of applications because large datasets and potent graphical processing units (GPUs) are readily available [26]. Moreover, recent work has investigated efficient DNN architecture synthesis. These architectural designs exhibit high computational efficiency in addition to high prediction accuracy [27,28]. Thus, researchers decided to use DNNs as AI Covid-19 diagnosis methods. This strategy has the advantages of efficiency and universal accessibility. AI is currently being used in the fight against Covid-19 in several ways [29]. Previous research has demonstrated that DL's enormous data handling capacity makes it one of the most promising technologies [30,31]. CNNs, which have demonstrated exceptional performance in speech, pattern, and image recognition, are the most well-known Deep learning technique. From the extracted relevant and usable features of the input images, they employ an end-to-end strategy to produce predictions. Due to its automatic feature extraction from the input image, CNN techniques outperform the conventional approach and are therefore increasingly popular among researchers for image classification. The results of previous study indicate that radiologists can work less when DL algorithms are used to identify Covid-19 on CXRs [24].

Early diagnosis is essential for the successful treatment for Covid-19 [32]. The assessment of CXRs is the most used diagnostic technique. Nonetheless, it is contingent upon the medical professional's interpreting skills and is typically not endorsed by other medical professionals. A fast, precise, and generalizable model is required to identify the condition. Current researchers choose to employ DL models (CNN), which automatically extract informative and relevant aspects of the input data to perform considerably better than traditional approaches that struggle with the relevant feature extraction from input images. While conventional NNs have demonstrated exceptional outcomes in Covid-19 identification and classification, they are not equipped to manage global information in intricate feature extraction. Enhancing the performance of the identification model can be achieved by integrating the global features of the data and expanding the receptive field of the neural network's feature extraction layer through the attention mechanism [33]. Relationships with distant pixels are therefore challenging to determine. To address this challenge, attention processes have been the subject of recent

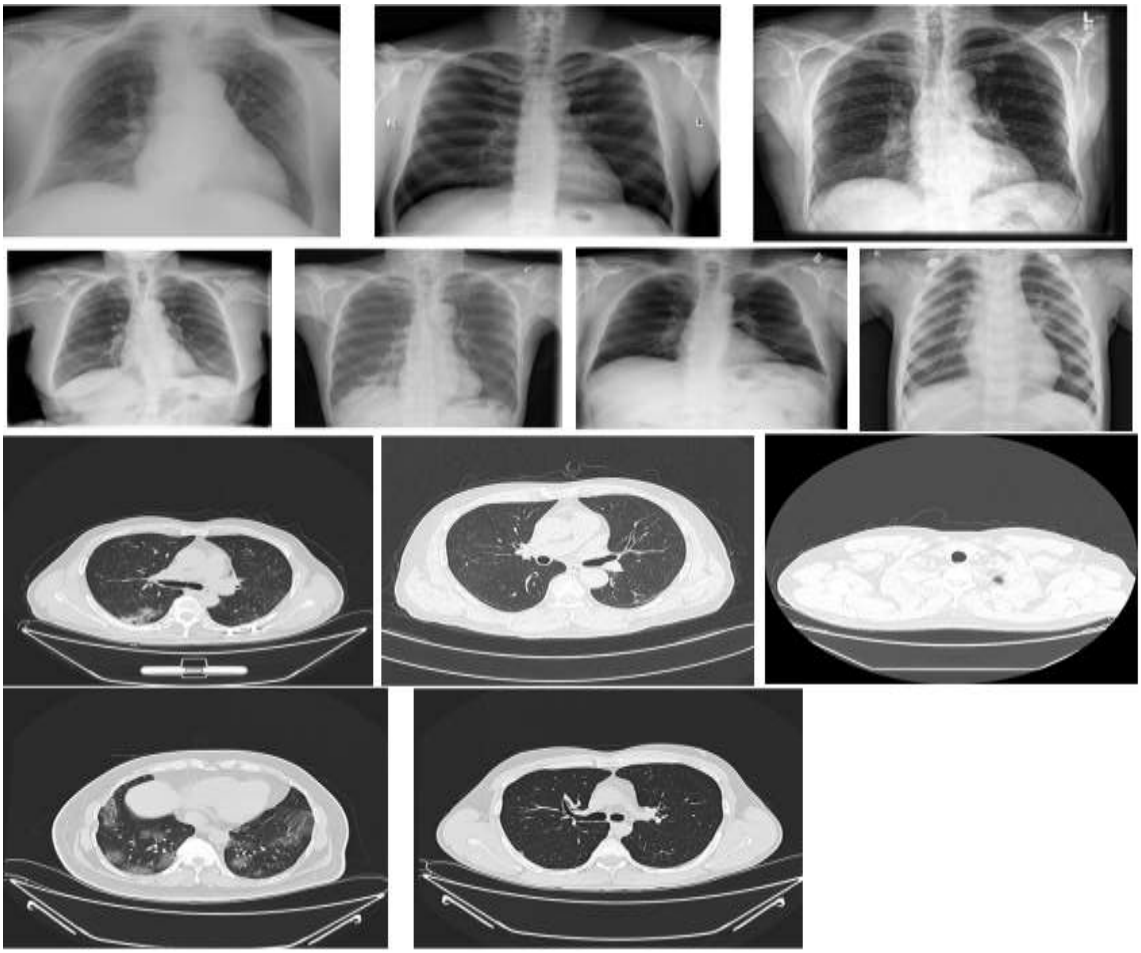

Figure 1. *Samples from each dataset. First row: Covid-19, Normal, Pneumonia (Left to right: x-ray dataset 1). Second row: Covid-19, lung opacity, normal, pneumonia (Left to right: x-ray dataset 2). Third row: pCT, nCT, NiCT (Left to right: CT dataset 1).*

attempts. Finding and focusing on the information that is most instructive within the data is done by using attention. Taking note of the shortcomings, this paper suggested a novel lightweight model as binary and multiclass classifier for lung opacity, pneumonia, and Covid-19 identification from CXRs and CT images. As has been recently done by numerous researchers for performance benefit, the proposed model may handle input raw images directly without any prior enhancement on the CXR and CT images [34,35]. Proposed model for Covid-19 classification is verified for accuracy and efficiency by performance analysis and comparison with the existing works.

The following summarizes the remaining portion of this work. Core contributions are described in Section 2. The dataset, materials, and proposed methodology are discussed in Section 3. The simulation environment is described in Section 4. Evaluation metrics, performance evaluation, and comparative analysis with existing works are discussed in Section 5. Discussion, strength and potential limitations, and conclusion are covered in section 6,7 and 8 respectively.

2. Main Contributions

We present a novel lightweight DL model based on the SqueezeNet architecture with the addition of attention mechanism in this study, to handle the classification into Pneumonia, Covid-19, Lung opacity, and normal categories, as well as the binary classification of Covid-19 categories. In addition to outperforming previous methods, our model makes numerous significant advances that highlight its importance in the field:

1) Using CXRs and CT images, we offer an efficient lightweight DL model to automatically detect Pneumonia, Lung Opacity and Covid-19.
2) Compared to numerous other studies that have been published in the literature, this one examines a different and larger CXR and CT datasets. These studies often focus on 2 and 3 class classifications and only comprise small number of CXR samples.
3) Our models significantly lower the processing power and memory requirements during the classification process when compared to the recent deep learning models published. They

also performed better than most of the current models in terms of accuracy rate.

4) After a thorough comparison with existing techniques, our proposed model seems to be more effective at identifying Pneumonia, Lung opacity and Covid-19 cases. This establishes our model as a practical and effective tool that can be used in clinical settings and helps with disease diagnosis.

3. Materials and Methods

3.1. Description of Datasets

In this work, different datasets are used to verify the performance of proposed model on CXR and CT images. 2,3, and 4 class classification tasks are performed on CXR images whereas 2, and 3 class classification tasks are performed on CT images. Images from each class from each dataset used in this study are shown in Fig.1. Description of each dataset is given below:

I. X-ray Dataset 1

CXR images from three different datasets [36], [37] and [38] were utilized to create this dataset. [36] consists of 1345, 10192, 6012, and 3616 images of Viral pneumonia, Normal, Lung opacity, and Covid-19 cases. CXR images of Covid-19 and Pneumonia classes from [37] and [38] respectively, are considered to enhance these classes in the dataset. The resulting dataset consists of total 28012 CXR images where 10000 Normal, 5909 Lung Opacity, 6500 Covid-19, and 5603 Pneumonia cases.

As indicated in Table 1, images were subsequently divided into three distinct sets at random: with 80:10:10 ratio for training, validation, and testing set. This serves to verify the suggested models' effectiveness in detecting Covid-19.

Table 1: *Split of X-ray Dataset 1.*

Class Label	Training	Validation	Testing	Total
Covid-19	5200	650	650	6500
Normal	8000	1000	1000	10,000
Pneumonia	4400	601	602	5603
Lung opacity	4809	550	550	5909
Total	22409	2801	2802	28012

II. X-ray Dataset 2

Instead of attempting data augmentation and image processing techniques explicitly, we have selected pre-processed version of the [36] dataset, which is proposed by Roy, S. et. al., 2022 [39] in their work and is publicly available. Authors utilizes advanced image processing and data augmentation techniques to create this dataset. There is total 7674 Lung opacity, 5365 Viral Pneumonia, 8745 Covid-19, and 8214 Normal images in the dataset. As shown in Table 2, the images were subsequently divided into three distinct sets at random: with 70:15:15 ratio for training, validation, and testing.

Table 2: *Split of X-ray dataset 2.*

Class	Training	Validation	Testing	Total
Covid	6121	1312	1312	8745
Normal	5749	1232	1233	8214
Viral Pneumonia	3755	805	805	5365
Lung opacity	5371	1151	1152	7674
Total	20,996	4500	4502	29,998

III. CT Dataset 1

Ning, W. et. al., 2020 [40] proposed this dataset. This dataset consists of data collected from two hospitals: Liyuan hospital and Union Hospital, China. This three-class dataset consists of 9979 Negative, 4001 Positive, 5705 Non informative CT images. Non informative CT images are those images in which no judgement can be made by lung parenchyma. As shown in Table 3, the dataset split was performed with 60:20:20 ratio for training, validation, and testing set.

Table 3: *Split of CT dataset 1.*

Class	Training	Validation	Testing	Total
Negative CT (nCT)	5987	1996	1996	9979
Positive CT (pCT)	2400	800	801	4001
Non informative CT (NiCT)	3423	1141	1141	5705
Total	11,810	3940	3938	19685

IV. CT Dataset 2

Islam, M. N. et. al., 2021 [41] proposed this dataset which is publicly available. 3840 non-Covid19 and 2242 Covid-19 images are present in this dataset. As shown in table 4,

the dataset split was performed with ratio of 60:20:20 for training, validation, and testing set.

Table 4: *Split of CT dataset 2.*

Class	Training	Validation	Testing	Total
Covid	1345	448	449	2242
Normal	2304	768	768	3840
Total	3649	1216	1217	6082

3.2. ECA Mechanism

Squeeze-and-excitation (SE) attention [42,43,44] can be optimized using fewer parameters with the use of the ECA model, which improves model performance. Additionally, attention mechanism ECA is a plug-and-play module [45]. Input feature map is first subjected to global average pooling in various channel dimensions by the ECA module, after which it is split into 1-D feature vector. Subsequently, a 1-D convolution kernel convolves the newly created feature vector, and the sigmoid activation function determines the new weight value. By multiplying by the initial input features, the new features are computed. This computation technique has the advantage of efficiently avoiding the channel dimension reduction issue and facilitating cross-channel feature information interaction [46], leading to an effective feature extraction procedure. The ECA module's structure is depicted in Fig 2.

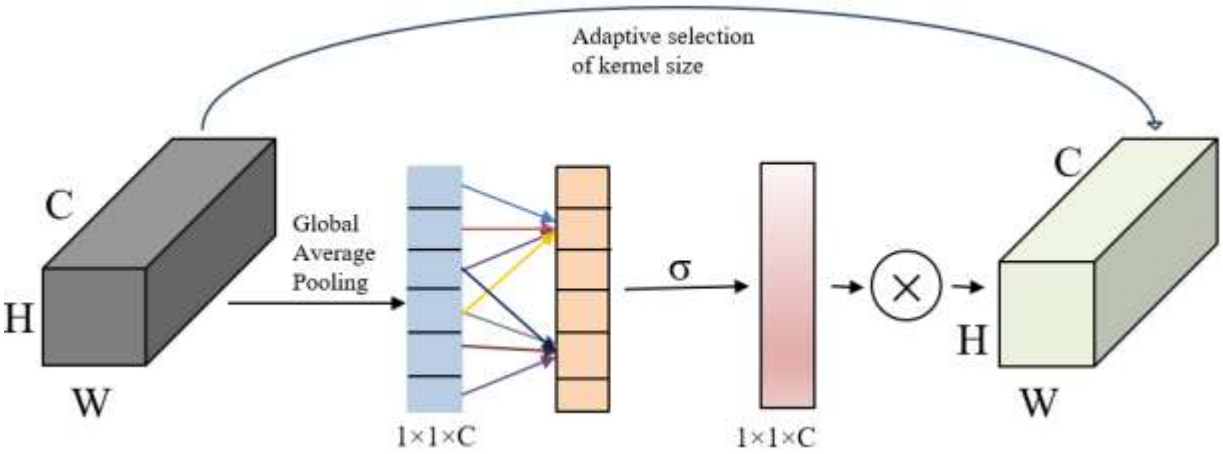

Figure 2. *Structure of ECA module.*

Same learning parameters are used by the ECA module on all channels to achieve cross-channel interaction during parameter learning [47]. Eq. (1) represents the expression for the process:

$$w_i = \sigma\left(\sum_{j=1}^{k} w^j y_i^j\right), y_i^j \epsilon \Omega_i^k \quad (1)$$

It should be noted that 1-D convolution with size k convolution kernel makes this parameter sharing method simple to implement. Eq. (2) represents the expression for the 1-D convolution process:

$$w = \sigma\left(C1D_k(y)\right) \quad (2)$$

Where sigmoid activation function is σ(.) and C1D(.) is a 1-D convolution. There is just k parameters used in the ECA module when utilizing this strategy.

To maximize the impact of feature extraction through cross-channel information interaction, it is crucial to choose appropriate interaction coverage, or the size of 1-D convolution kernel [48]. CNN design frequently has disparate numbers of channels in output features of different locations. Computational complexity and resources are significant if the ideal cross-channel interaction coverage appropriate for various channel numbers is achieved by hand-adjusting the convolution kernel's size. An adaptive convolution kernel size estimation technique that works with various channel dimensions was presented by Wang et al., 2020 [46]. A 1-D convolution kernel size k that is adaptable given the number of channels C. C and k are mapped as in Eq. (3):

$$C = \phi(k) \quad (3)$$

One popular and basic mapping connection is mapping of a linear connection, as in Eq. (8). But, due to its oversimplification, linear mapping will frequently be constrained and unable to satisfy the true requirements. The channel dimension C in CNN parameters are typically a power of 2. To produce a nonlinear mapping function, as indicated by Eq. (5), the original linear function Eq. (4) is enhanced.

$$\phi(k) = \gamma \times k - b \quad (4)$$

$$C = \phi(k) = 2^{(\gamma \times k - b)} \quad (5)$$

The size of the 1-D convolution kernel k is determined by the number of channels C, as shown in Eq. (6):

$$k = \Psi(C) = \left| \frac{\log_2(C)}{\gamma} + \frac{b}{\gamma} \right|_{odd} \quad (6)$$

If b is set to 1 and γ is set to 2, and |t| is odd integer that is closest to t. Eq. (10) mapping connection suggests that higher-dimensional channels require convolution kernels of larger size to accommodate cross-channel interactions. In contrast, a smaller convolution kernel is determined by low-dimensional channel to complete a restricted set of interactions.

3.3. Proposed System

With fifty times less parameters than Alexnet, SqueezeNet is a CNN that performs better [35,42,43]. There are fifteen layers in SqueezeNet: 2 convolution layers, 3 max pooling layers, 8 fire modules, 1 global average pooling layer, and 1 output layer SoftMax. Fig. 3 shows the design of the proposed lightweight model for Covid-19 classification. This model performs binary and multiclass classification tasks. Except for classification layer, the hidden layers for feature extraction are same for 2,3, and 4 class classification tasks. The aim of our work is to maintain state-of-the-art performance at a lower computational and memory cost. This is helpful in scenarios where the model must be installed on devices with limited resources, like embedded systems or mobile phones. Lightweight models are also easier to use in practical applications because they are quicker to train and predict.

CNN does not require human intervention to identify the distinctive elements of the image; instead, it can quantify the image's features layer by layer. Enhancing the model's performance and refining the neural network's structure take on additional dimensions with the addition of an attention module. Enhancing the network model's performance with low computational cost for Covid-19 classification is the aim of this study. Inspired from the SqueezeNet architecture, our proposed model consists of 2 Convolutional layer, 1 ECA module, 1 BatchNormalization, 6 Fire modules, 5 Maxpooling layers, 1 GlobalAveragePooling and 1 classification layer. BatchNormalization is used in our proposed model to normalize the output of the ECA module. Maxpooling layer is applied after each fire module except the last to reduce the dimensionality of the fire module's output. ECA is applied to the 1st convolution layer in fire module then the output of ECA is forwarded to the convolution layer of 1×1 and convolution layer of 3×3. Then the output of these two-convolution layer is concatenated. Squeeze and expand size of each modified fire module in the proposed model is shown in Table 6. The layer wise description of the proposed model is illustrated in Table 5. It can be seen from the Table that our proposed model has approx. 571k number of parameters whereas original SqueezeNet model [35] has 1,248,424 number of parameters. The size of our proposed model is 2.18 MB whereas original SqueezeNet model has size of 4.8 MB.

Table 5. *Layer-wise architecture of proposed model (for binary classification).*

Type of layers		Output Shape	Param#
Input layer	-	(128,128,1)	0
Conv2d	-	(64,64,64)	9,472
ECA layer	-	(64,64,64)	3
BatchNormalization	-	(64,64,64)	256
Fire 1	Conv2d	(64,64,16)	1,040
	ECA layer	(64,64,16)	3
	Conv2d	(64,64,64)	1,088
	Conv2d	(64,64,64)	9,280
	Concatenate	(64,64,128)	0
MaxPooling2d	-	(32,32,128)	0
Fire 2	Conv2d	(32,32,16)	2,064
	ECA layer	(32,32,16)	3
	Conv2d	(32,32,64)	1,088
	Conv2d	(32,32,64)	9,280
	Concatenate	(32,32,128)	0
MaxPool2d	-	(16,16,128)	0

Fire 3	Conv2d	(16,16,32)	4,128
	ECA layer	(16,16,32)	3
	Conv2d	(16,16,128)	4,224
	Conv2d	(16,16,128)	36,992
	Concatenate	(16,16,256)	0
MaxPool2d	-	(8,8,256)	0
Fire 4	Conv2d	(8,8,48)	12,336
	ECA layer	(8,8,48)	3
	Conv2d	(8,8,192)	9,408
	Conv2d	(8,8,192)	83,136
	Concatenate	(8,8,384)	0
MaxPool2d	-	(4,4,384)	0
Fire 5	Conv2d	(4,4,64)	24,640
	ECA layer	(4,4,64)	3
	Conv2d	(4,4,256)	16,640
	Conv2d	(4,4,256)	147,712
	Concatenate	(4,4,512)	0
Maxpool2d		(2,2,512)	0
Fire 6	Conv2d	(2,2,64)	32,832
	ECA layer	(2,2,64)	3
	Conv2d	(2,2,256)	16,640
	Conv2d	(2,2,256)	147,712
	Concatenate	(2,2,512)	0
Conv2d		(2,2,2)	1026
GobalAveragePool2d		(2)	0
Activation		(2)	0

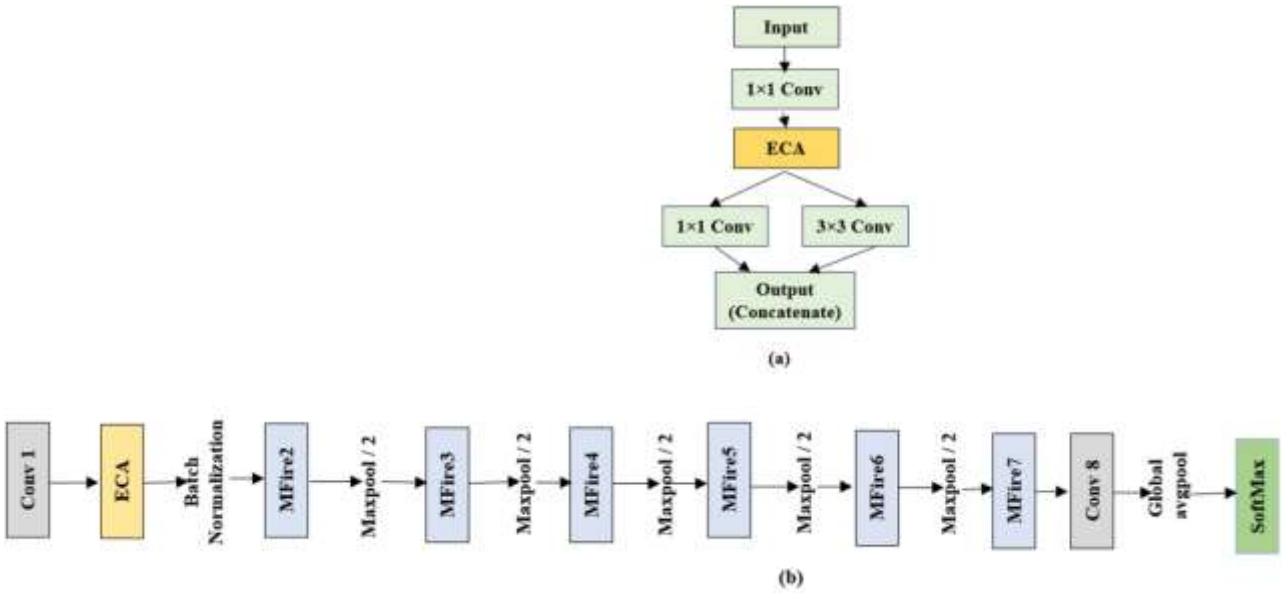

Figure 3. *(a) Proposed Fire module (b) Proposed model based on SqueezeNet architecture.*

Table 6. *Modified Fire (MFire) modules.*

Module (MFire)	Squeeze size	Expand size
MFire 2	16	64
MFire 3	16	64
MFire 4	32	128
MFire 5	48	192
MFire 6	64	256
MFire 7	64	256

To handle unstable gradients, expedite model learning, and solve overfitting issue, batch normalization is employed for many reasons. We have used batch Normalization in our proposed network to normalize the output of the attention layer.

$$y^* = \frac{x - E[y]}{sqrt(var(y))} \quad (7)$$

The new value is indicated by y* in the Eq. (7), the variance of y with a batch is indicated by var(y), and the mean value of y with a batch is indicated by E(y). To reduce dimensionality and downscale the images, the max-pooling layer also known as sub-sampling is employed. This lowers overall expenses and processing effort. A max pooling operation is applied to a convolutional layer's output, selecting the highest value from a range of contiguous input values.

4. Experimental Setup

Our suggested approach is comparatively straightforward, requiring minimal preparation and capable of handling collection of imaging dataset without any advanced image preprocessing and enhancement techniques. Unlike many other approaches, ours does not require any specific manipulation of the dataset, nor does it involve the generation of any dynamic or static features. For experimental purpose, we employed TensorFlow with keras library, Scikit-Learn, and Python 3.5 on Google Colab.

Attention mechanism helps the neural network to attain the region of interest resulting better model performance and generalizability. ECA mechanism is used in our proposed model. Each Max-pool 2D layer used in the model have kernel size of 3 and strides of 2 with padding same. For binary and multiclass classification during training, the binary and categorical cross entropy losses were applied, respectively. Using a specific optimization approach to lower the prediction error, the model can be made to perform better over time by measuring the difference between true values and the values predicted by the model. Eq. (8) and (9) provide a mathematical expression for the losses.

Table 7. *Parameters summary for proposed model.*

Hyperparameters	Value
Input shape	(128,128,1)
Rate (Learning)	0.0001
Function (Loss)	Binary and Categorical cross entropy
Functions (Activation)	ReLU, Sigmoid, SoftMax
Functions (Activation)	Adam
Performance metrics	Recall, f1-score, precision, and accuracy

$$L_{BL}(p,q) = -\frac{1}{n}\sum_{i=1}^{n} p_i \log(q_i) + (1-p_i)\log(1-q_i) \quad (8)$$

$$L_{CCL}(p,q) = -\frac{1}{n}\sum_{i=1}^{n}\sum_{j=1}^{c} p_{i,j}\log(q_{i,j}) \quad (9)$$

Where, number of classes = c, number of samples (CXR/CT images) used = n, and p_i and q_i represent the samples' true and predicted values respectively. The binary and categorical cross-entropy losses are represented by L_{BL} and L_{CCL}, respectively.

The training parameter used for training purpose were: 32 batch size, 100 epoch, 0.0001 learning rate. Activation function is ReLU that is employed, except for the output layer, where Sigmoid is used for binary and SoftMax activation is used for multi class classification. Using Adam optimizer, binary and categorical cross-entropy loss for two and multiclass classification respectively, the model is compiled. Table 7 presents a summary of the hyperparameters used to train our proposed model. It is shown that the input images with the input shape (128,128,1) and the binary and categorical cross entropy loss function were utilized in the implementation.

5. Results and Discussion

Results of applying the proposed model for 2,3, and 4 classes are computed as well as displayed. Following training, validation, and testing, the model's performance for each class is assessed using the f1 score, confusion matrix, accuracy, precision, and recall. The ratio of the total number of images that the model successfully classified to the total number of images was used to compute the suggested approach's accuracy (Eq. 10).

$$Accuracy = \frac{Correlctly\ classified\ number\ of\ images}{total\ images} \quad (10)$$

Additionally, f1-score (Eq. 13), recall (Eq. 11), precision (Eq. 12) are used to verify the performance of proposed model:

Recall (Sensitivity): The metric used to assess a predictive model's sensitivity is called Recall (Rec). It calculates the percentage of positive occurrences that are expected to be positive. Typically, it is written as follows: where T_p denotes true positive and F_n denotes false negative.

$$Recall = \frac{Tp}{Tp+Fn} \times 100 \quad (11)$$

Precision (Prec): This is an additional performance metric included in the research. It is described as model's performance of "True Positive" (T_p) findings. It is put as in (Eq. 15):

$$Precision = \frac{Tp}{Tp+Fp} \times 100 \quad (12)$$

Where F_p stands for false positive and T_p for true positive.

F1-score: A statistic called the F1-score (Eq. 16) describes the stability between Rec and Prec. It is the Prec and Rec harmonic average.

$$F1 - score = 2 \times \frac{Recall \times Precision}{Recall + Precision} \quad (13)$$

Table 8. *Performance on X-ray dataset 1 for 3 class classification.*

Class	Recall	Precision	Accuracy	F1-score
Covid	.9635	.9738	.9686	.9814
Normal	.9818	.9730	.9774	.9795
Pneumonia	.9620	.9635	.9637	.9818

Table 9. *Performance on X-ray dataset 1 for 4 class classification.*

Class	Recall	Precision	Accuracy	F1-score
Covid	.9347	.9462	.9722	.9404
Normal	.9456	.9380	.9586	.9418
Lung opacity	.9255	.9286	.9686	.9270
Pneumonia	.9234	.9200	.9693	.9217

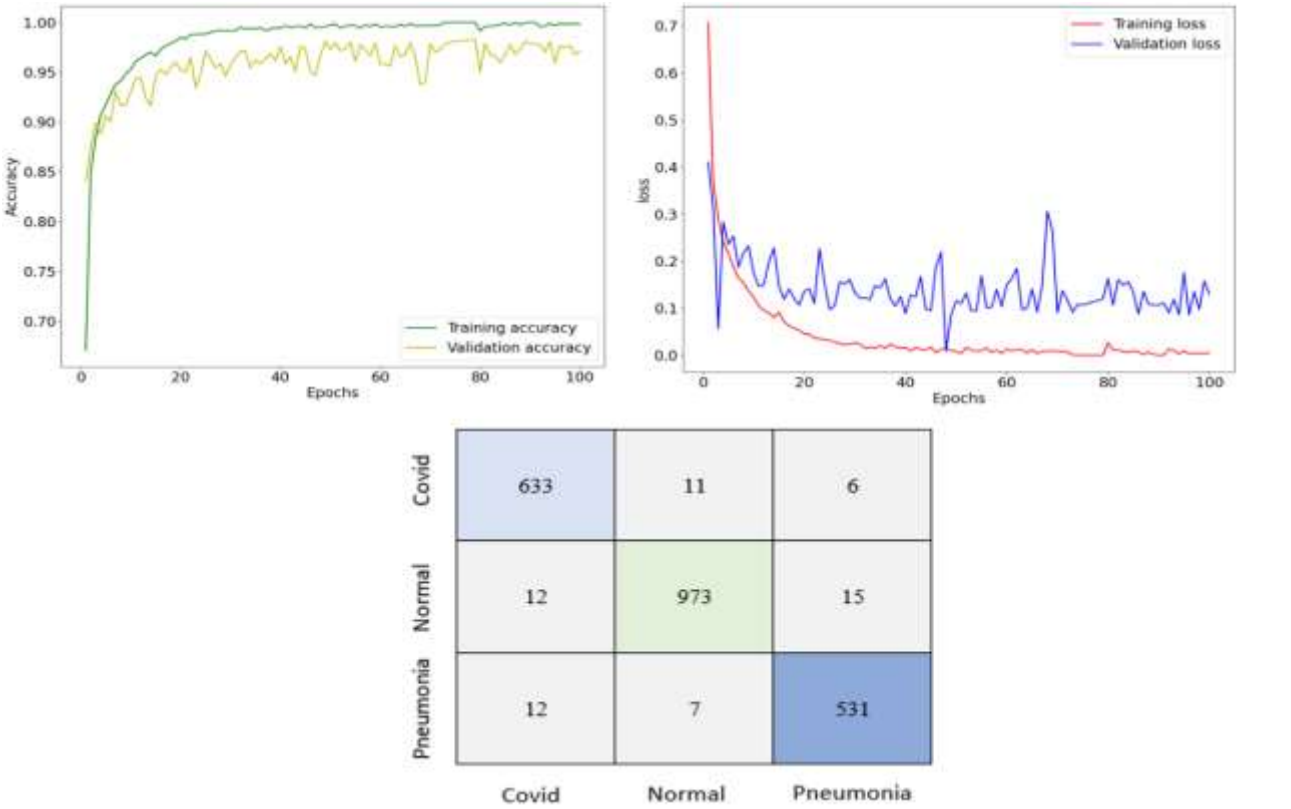

Figure 4. *Training/validation accuracy and loss curves and confusion matrix on test set for X-ray dataset 1 for 3 class classification.*

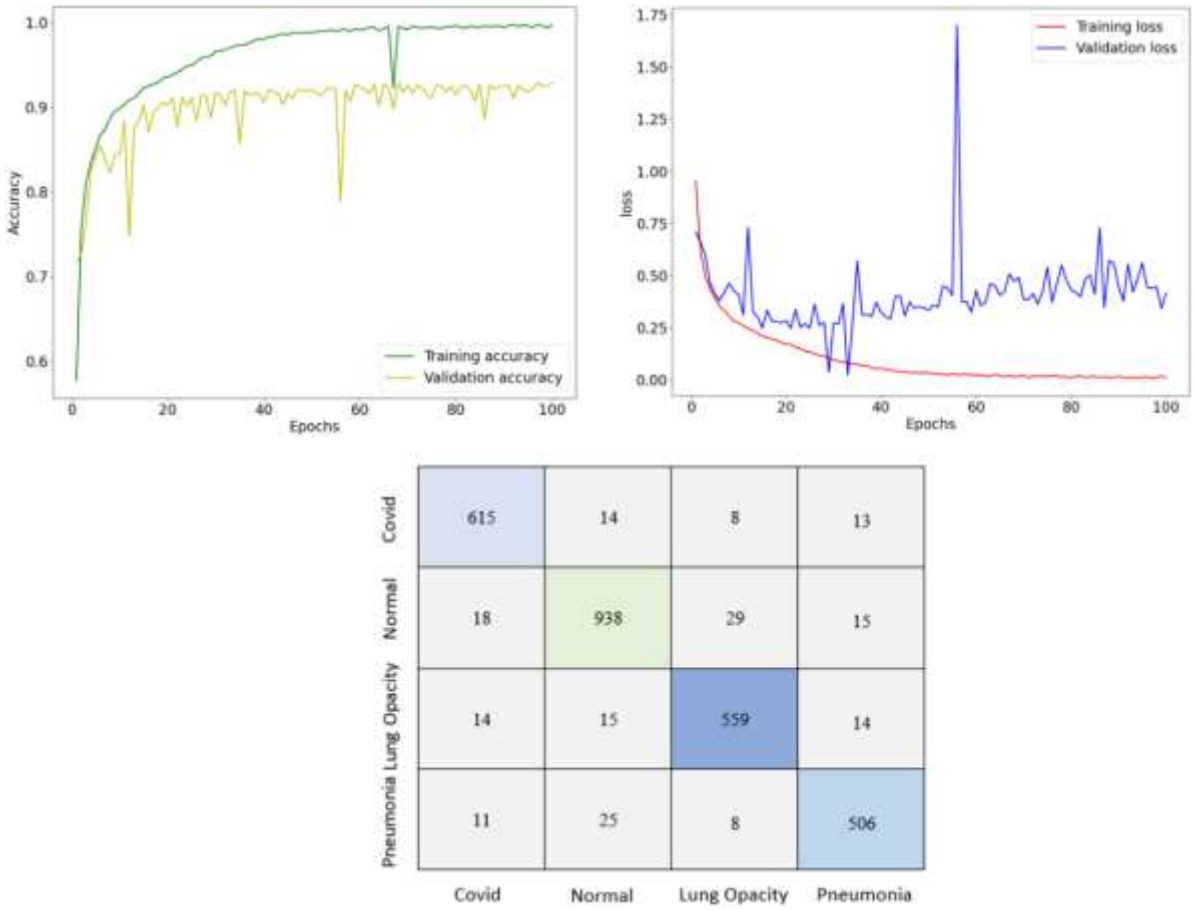

***Figure 5**. Training/validation accuracy and loss curves and confusion matrix on test set for X-ray dataset 1 for 4 class classification.*

***Table 10.** Performance on X-ray dataset 2 for 2 class classification.*

Class	Recall	Precision	Accuracy	F1-score
Covid	.9977	.9954	.9965	.9966
Normal	.9951	.9976	.9965	.9964

***Table 11.** Performance on X-ray dataset 2 for 3 class classification.*

Class	Recall	Precision	Accuracy	F1-score
Covid	.9825	.9825	.9863	.9825
Normal	.9814	.9854	.9878	.9834
Pneumonia	.9850	.9789	.9913	.9819

***Table 12.** Performance on X-ray dataset 2 for 4 class classification.*

Class	Recall	Precision	Accuracy	F1-score
Covid	.9826	.9886	.9916	.9856
Normal	.9967	.9951	.9978	.9959
Lung opacity	.9836	.9987	.9929	.9861
Pneumonia	.9874	.9727	.9929	.9800

***Table 13.** Performance on CT dataset 2 for 2 class classification.*

Class	Recall	Precision	Accuracy	F1-score
Covid	.9956	.1.00	.9984	.9978
Normal	1.00	.9974	.9984	.9987

***Table 14.** Performance on CT dataset 1 for 3 class classification.*

Class	Recall	Precision	Accuracy	F1-score
nCT	.9980	.9970	.9975	.9975
pCT	.9864	.9925	.9957	.9894
NiCT	.9938	.9912	.9957	.9925

5.1. Performance on X-ray Datasets

This study uses two X-ray datasets to verify how well the proposed model performs on CXR images. X-ray dataset 1 is the collection of multiple publicly available datasets. This dataset is used to perform classification tasks for 3 and 4 classes. Table 8 and 9 represents the class-wise performance for 3 and 4 classes. One can observe from these tables that proposed model performed well with the precision

of 97.38% with 96.86% accuracy for Covid-19 class in 3 class classification task and 94.62% precision score with 97.22% accuracy for Covid-19 class in 4 class classification tasks. The misclassification rate of 0.0286 and 0.0657 for 3 and 4 classes respectively on X-ray dataset 1 show its superior performance and represents that how effectively the proposed model can identify the images correctly. Fig. 4 and Fig. 5 represent accuracy and loss curves on training/validation set along with the confusion matrix for test set for 3 and 4 class classification tasks respectively on X-ray dataaset1.

X-ray dataset 2 is another dataset for performance verification of proposed model. It is an augmented and pre-processed dataset proposed by Roy, S. et al., 2022 [39] and is publicly available. The proposed model is performing exceptionally well on this dataset. The proposed model's performance on 2,3, and 4 class classification tasks is shown class-wise in tables 10,11, and 12. 99.54% precision with 99.65% accuracy for Covid-19 class in 2 class scenario, 98.25% precision with 98.63% accuracy for Covid-19 class in 3 class scenario, and 98.86% precision with 99.16% accuracy for Covid-19 class in 4 class scenarios show the exceptional performance of proposed model when the advanced pre-processing techniques are applied on dataset.

The performance metrics show that the proposed model is performing well when the X-ray dataset is augmented and pre-processed. But without the use of data augmentation and advanced image preprocessing techniques, proposed model proved its superior performance over the existing models.

The comparative study of proposed model with the current studies is presented in Tables 15. Roy, S. et al., 2022 [39] proposed the X-ray dataset 2 used in this study. It can be noticed from the Table 14 that their proposed model "ResNet50+SVD-CLAHE Boosting +BWCCE" got 94% accuracy for 4 classes with 1,019,396 trainable parameters whereas our proposed model got 98.76% accuracy for 4 classes on same dataset with only approximate 571k parameters. For 2 class classification task, total 16959 CXR images are employed where 8745 Covid-19 and 8214 Normal images. With large amount of CXR images, our proposed model performs exceptionally well with 99.64% accuracy which is greater than the existing studies reported in this paper. Fig. 6, 7 and 8 represent accuracy and loss curves on training/validation set and confusion matrix for test set for 2,3 and 4 class classification tasks on X-ray dataset 2. Fig.9,10 and 11 shows the comparison among the F1-score reported by the proposed model on Xray dataset 1 and 2 and existing works for 2,3 and 4 class classification on CXR images. Roy, S. et al., 2022 [39] reported a F1-score of 95 on X-ray dataset 2 whereas our proposed model got a F1-score of 98.76. Pradeep Dalvi et al., 2024 [55] proposed the lightweight model with only 2,00,034 parameters got 98.47% accuracy for 2 class classification with total of 13,808 CXR images where only 3616 images belong to Covid-19 class. Ainapure, B. S. et al., 2024 [56] proposed the lightweight model with only 511,650 parameters got 99% accuracy for 2 class classification with total of 2940 CXR images where

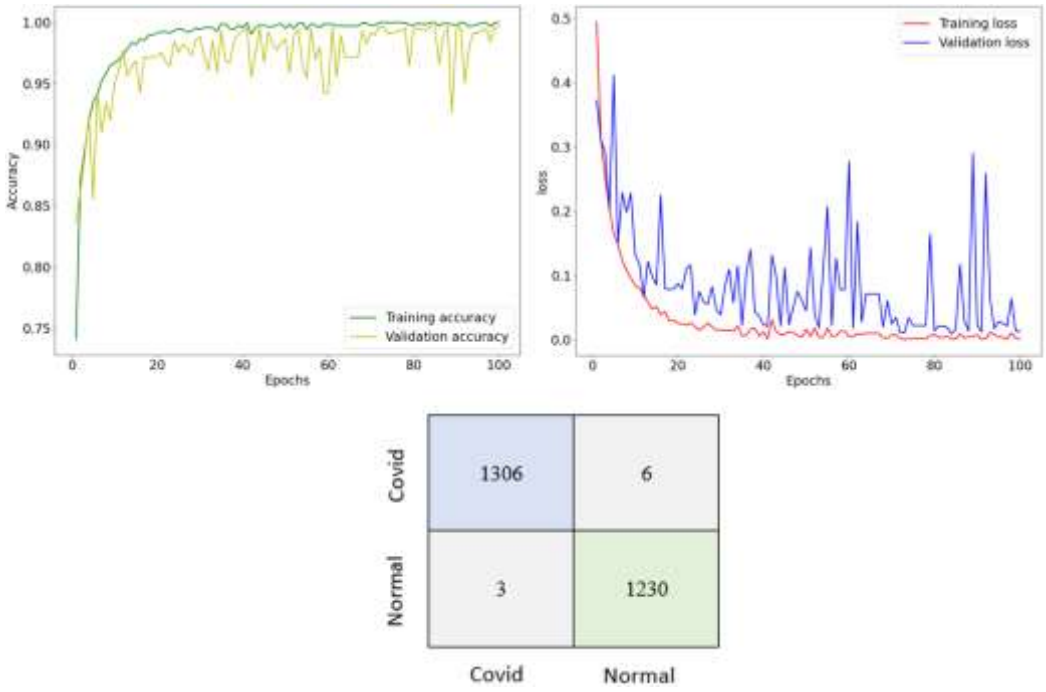

Figure 6. *Training/validation accuracy and loss curves and confusion matrix on test set for X-ray dataset 2 for 2 class classification.*

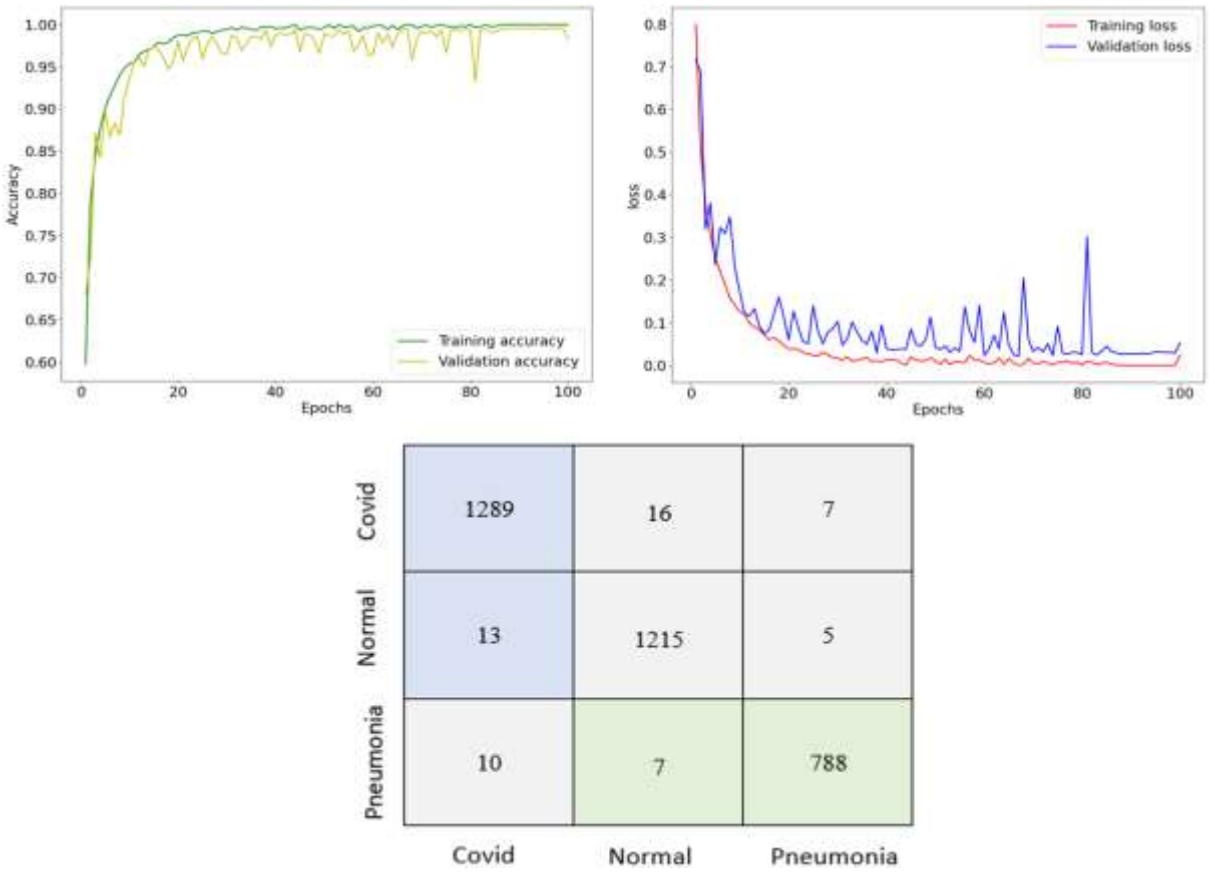

Figure 7*. Training/validation accuracy and loss curves and confusion matrix on test set for X-ray dataset 2 for 3 class classification.*

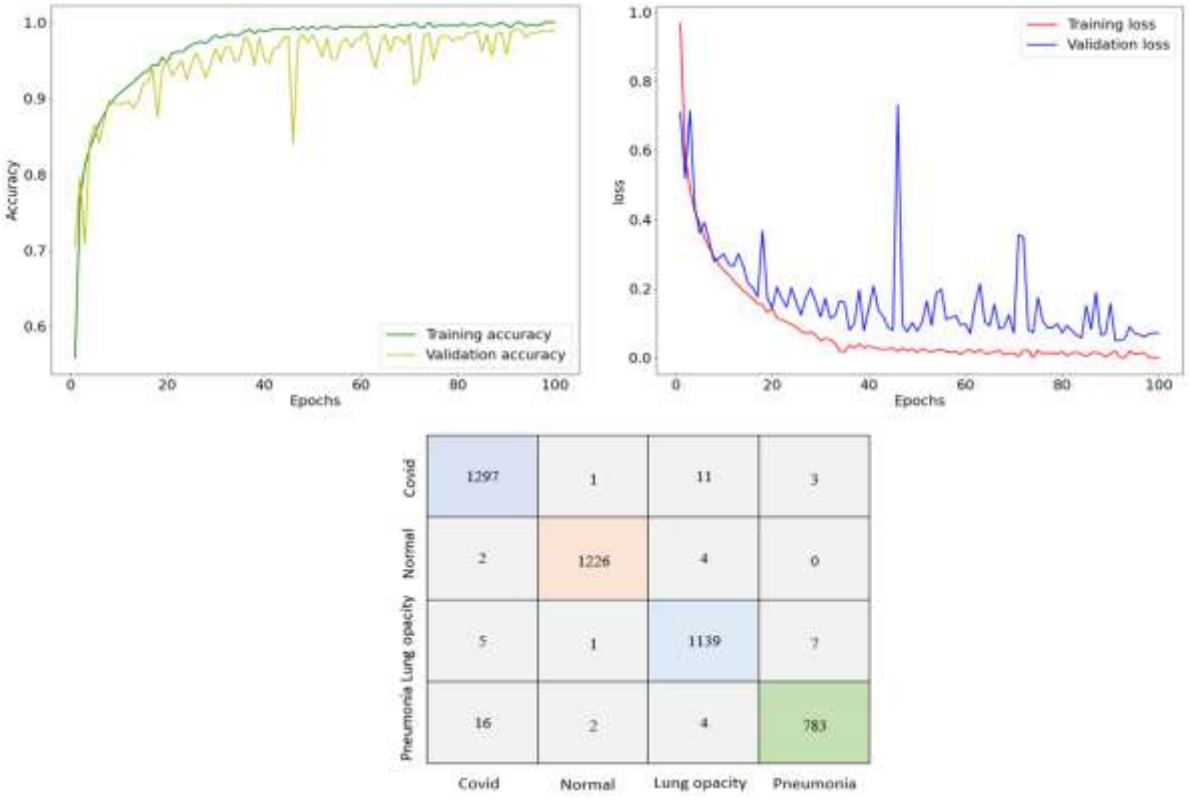

Figure 8. *Training/validation accuracy and loss curves and confusion matrix on test set for X-ray dataset 2 for 4 class classification.*

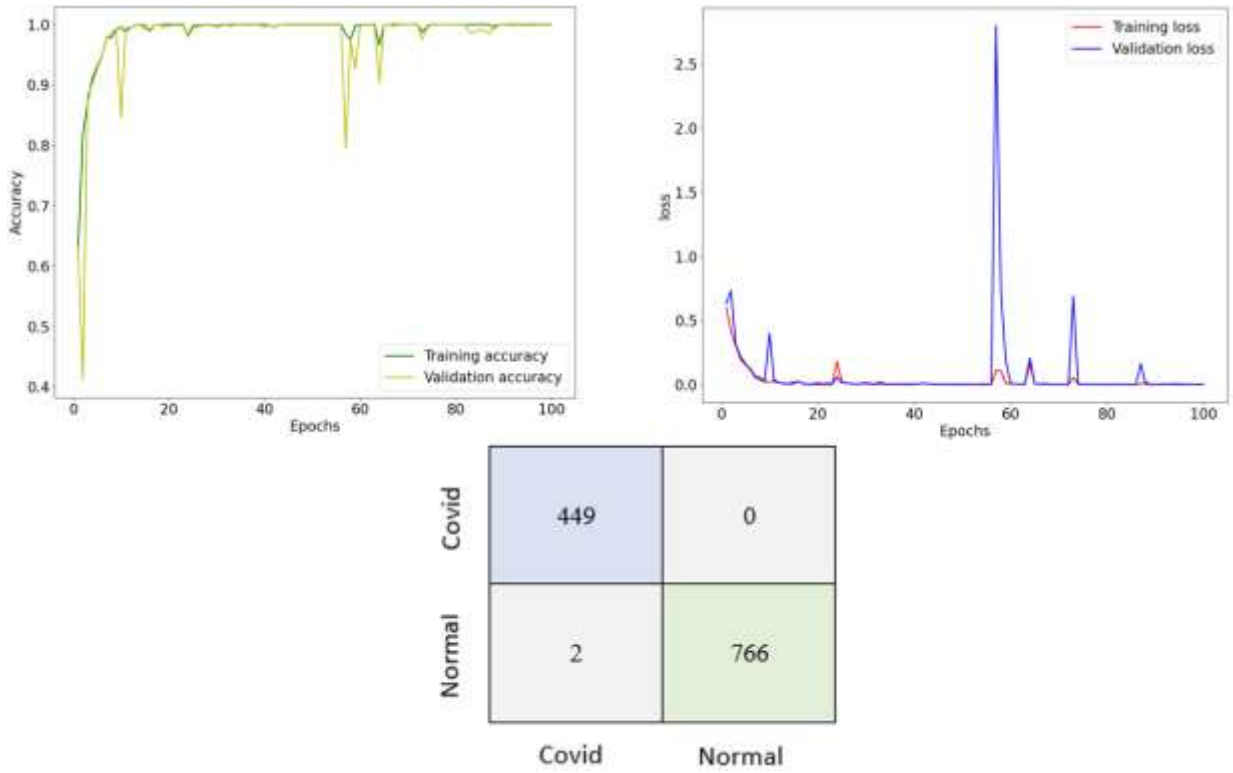

Figure 9. *Training/validation accuracy and loss curves and confusion matrix on test set for CT dataset 2 for 2 class classification.*

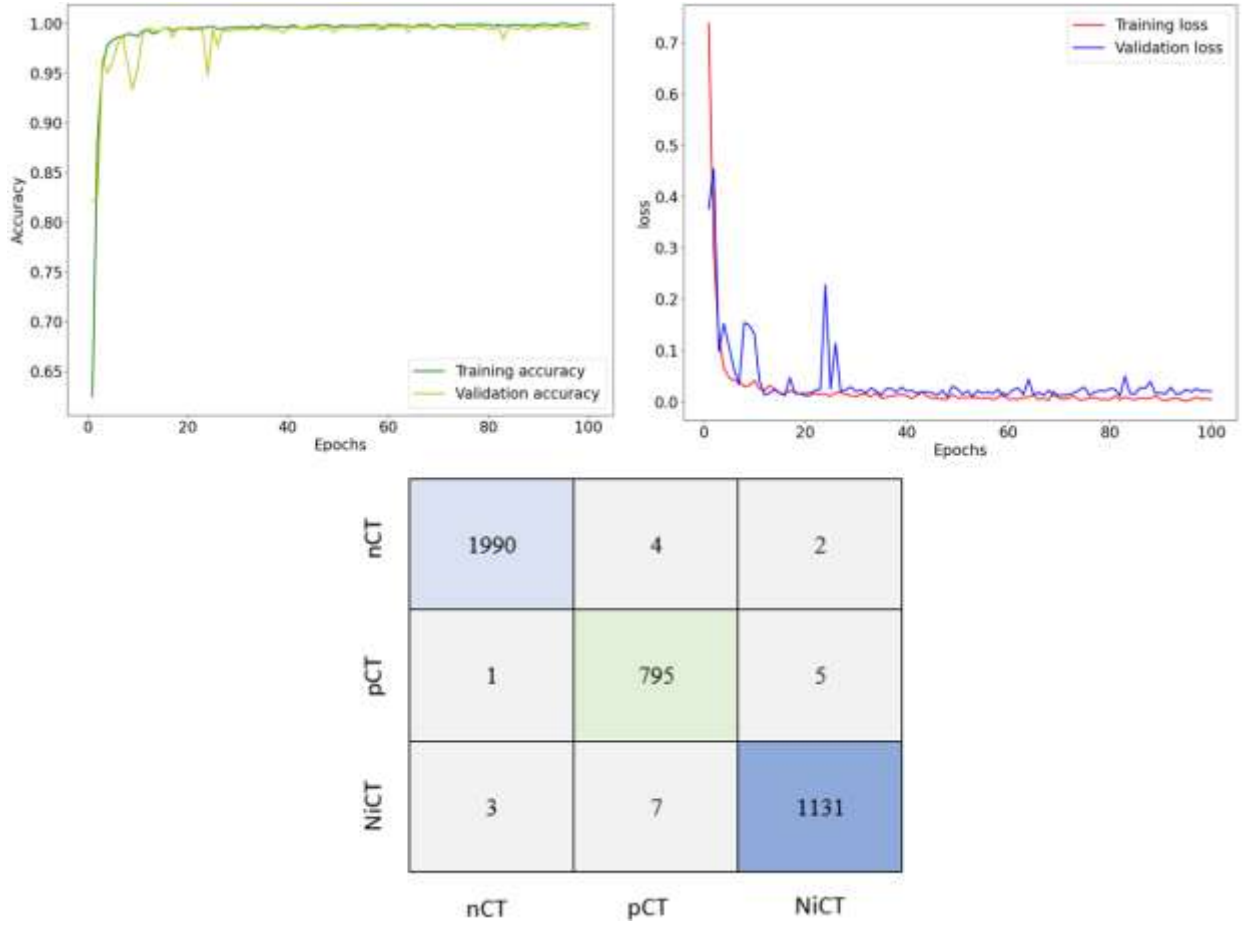

Figure 10. *Training/validation accuracy and loss curves and confusion matrix on test set for CT dataset 1 for 3 class classification.*

Table 15. *Comparative analysis of our proposed model with current classification models in terms of parameters and accuracy on X-ray datasets.*

References	Architecture	Dataset	Classes	Accuracy	Parameters
George, G.S. et al.,2023 [49]	GrayVIC model	Covid-19 = 2250, Normal = 2250	2	98.06%	2,684,650
		Covid-19=2250, Normal=2250, Pneumonia=2250	3	97.41%	2,684,650
Jyoti, K et al.,2023 [50]	ResNet50	Covid-19 = 2409, Normal = 2866	2	95.67%	23,591,810
Malik, D. et al.,2022 [51]	VGG16	Covid-19 = 4630, Normal = 1583	2	93.00%	14,715,714
Ukwandu, O. et al.,2022 [52]	MobileNet-V2	Covid-19 = 1200, Normal = 1341	2	99.60%	3,538,984
		Covid-19=1200, Normal=1341, Pneumonia=1345	3	94.50%	3,538,984
Nayak et al.,2022 [53]	LW-CORONet	Covid-19 = 2358, Normal = 8066	2	96.25%	680,000
		Covid-19=2358, Normal=8066, Pneumonia=5575	3	95.67%	
Hussein, H.I. et al., 2023 [54]	CNN	Covid-19=3616, Normal=10192	2	98.55%	591,903
		Pneumonia=1345, Normal=10192, Covid-19=3616	3		592,929
Pradeep Dalvi et al., 2024 [55]	Proposed method	Covid-19=3616, Normal=10192	2	98.47%	2,00,034
Ainapure, B. S. et al., 2024 [56]	Proposed method	Covid-19(+) =1364, Covid-19(-) =1576	2	99%	511,650
Wang, S. et al., 2024 [57]	Dense MobileNetV3	Pneumonia=1345, Normal=10192, Covid-19=3616	3	98.71%	5,948,169
Asif, S. et al ., 2024 [58]	LWSE	Normal=890, Pneumonia=892, Covid-19=900	3	96.40%	4,05,0000
		Normal=1349, Pneumonia=1345, Covid-19=1361, Tuberculosis=1300	4	97.89%	4,25,0000
Huang, M. L. et al., 2022 [59]	Lightweight EfficientNetV2	Covid-19=600, Normal=600, Pneumonia=600	3	98.33%	798,539
Ahamed, K. U. et al., 2021 [60]	Modified & Tuned ResNet50V2	Covid-19=1143, Normal=1150, Pneumonia=1150	3	97.24%	49,210,756
Sanida, T. et al., 2022 [61]	Modified MobileNetv2	Viral pneumonia = 1245, Lung opacity = 6012, Normal = 10192, COVID-19 = 3616	4	95.80%	2,915,908

Roy, S. et al., 2022, [39]	ResNet-50+SVD-CLAHE Boosting +BWCCE	Covid-19=8769, Normal=8192, Lung opacity=7662, pneumonia= 5410	4	94%	1,019,396
Asham, M. A. et al., 2024 [62]	Proposed KD Student Model	Covid-19=1316 Normal=1341 Pneumothorax=1348 Tuberculosis=1300	4	94.43%	630000
Proposed work	Proposed CNN	X-ray Dataset 2 Healthy=8214, Covid-19=8745	2	99.64%	571,015
		X-ray dataset 1 Healthy=10000, Pneumonia=5500, Covid-19=6500	3	97.13%	571,528
		X-ray dataset 2 Healthy=8214, Pneumonia=5365, Covid-19=8745	3	98.27%	
		X-ray dataset 1 Normal = 10000, Lung Opacity = 6012, Viral Pneumonia = 5500, Covid-19 = 6500	4	93.43%	572,041
		X-ray Dataset 2 Normal = 8214, Lung Opacity = 7674, Viral Pneumonia = 5365, Covid-19 = 8745	4	98.76%	

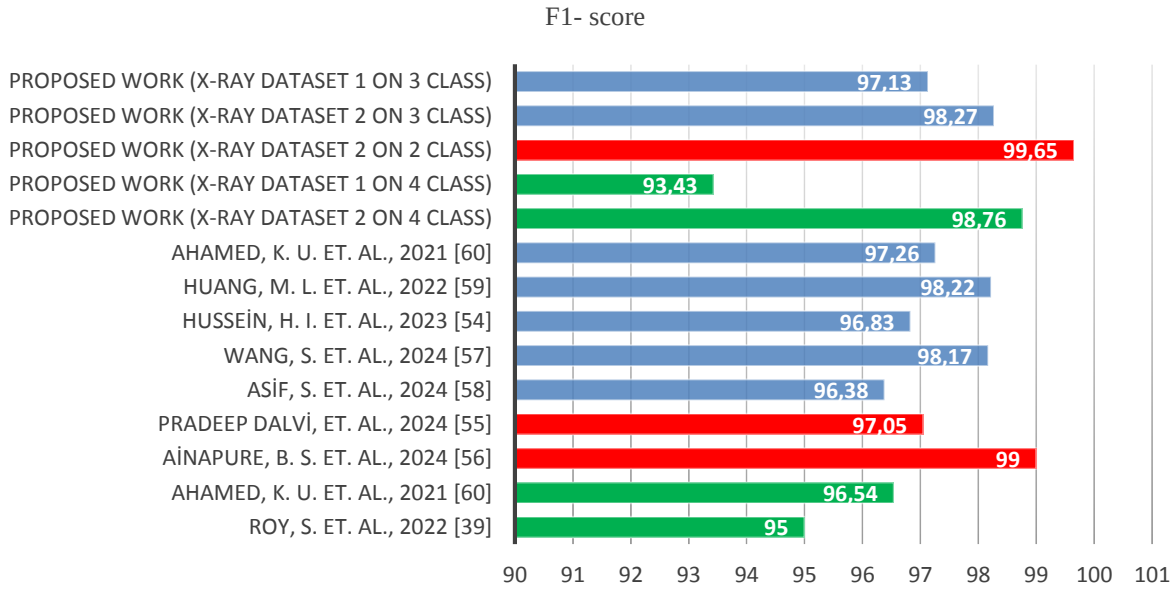

Figure 11. *Comparison of F1-score on X-ray dataset: Proposed work vs Recent works (Red: 2 class, Blue: 3 class, Green: 4 class).*

Table 16. *Comparative analysis of our proposed model with current classification models in terms of parameters and accuracy on CT dataset.*

References	Architecture	Dataset	Classes	Accuracy	Parameters
Asif, S. et al., 2024 [63]	LitefusionNet	Covid-19=1200, Normal=1200	2	99.00%	6,67,0000
Soleimani-Fard, S. et al., 2024 [64]	Res-MGCA-SE	Covid-19=349, Normal=397	2	93.42%	5,50,0000
Ahamed, K. U. et al., 2021 [60]	Modified & Tuned ResNet50V2	Covid-19=1000, Normal=1000, CAP images=1000	3	99.01%	49,210,756
Huang, M. L. et al., 2022 [59]	Lightweight EfficientNetV2	Covid-19=600, Normal=600, Pneumonia=600	3	97.48%	798,539
Asif, S. et al., 2024 [58]	LWSE	Covid-19=1200, Normal=1200	2	98.83%	3,85,0000
Proposed work	Proposed CNN	CT dataset 1 Covid-19=2242, Normal=3840	2	99.84%	571,015
		CT dataset 2 Negative CT=9979, Positive Ct=4001, Non-informative CT=5705	3	99.44%	571,528

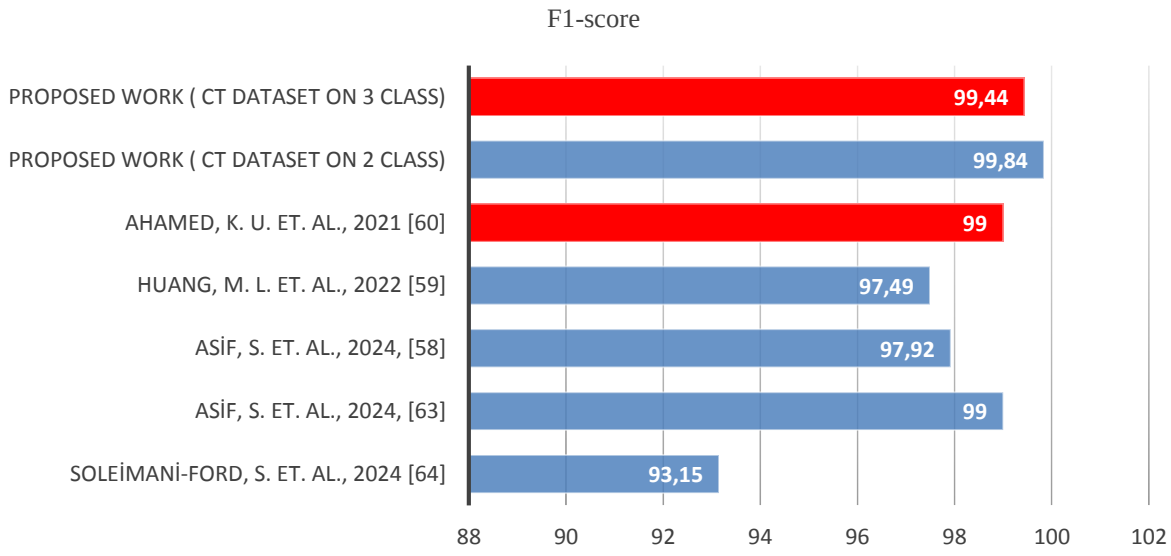

Figure 12. *Comparison of F1-score on CT dataset: Proposed work vs Recent works (Blue: 2 class, Red: 3 class).*

only 1364 images belong to Covid-19 class. These beforementioned studies have neither incorporated larger datasets as ours nor performed the multiclass classification. Our proposed model got 99.64% accuracy for 2 class classification with total of 16959 CXR images where 8745 images belong to Covid-19 class which is also greater than these beforementioned studies.

5.2. Performance on CT Datasets

Most of the existing studies reported lightweight models on CXR images for Covid-19 classification. Very few proposed the lightweight model for Covid19 classification on CT images or CT and CXR images both. Proposed model in this study performed the 2 and 3 class classification tasks on

CT images. Table 13 and 14 shows the class-wise performance on CT dataset for 2 and 3 class classification tasks. For 2 class classification, precision score of 100% with 99.84% accuracy for Covid-19 class represents the remarkable performance of the proposed model on CT dataset. Whereas 99.25% precision score with 99.57% accuracy for covid-19 class represent the superior performance of the proposed model for 3 class classification tasks. The misclassification score of .0056 and .0016 for 2 and 3 class classification tasks show that model is performing well in

Table 17. *Comparative analysis of proposed model in terms of accuracy and computational cost with most current studies.*

References	Accuracy	Class	Number of test images	Parameters	Test time	Model size
Asham, M. A. et al., 2024 [62]	94.43%	4	1276 CXR	630000	11.41s	2.66 MB
Asif, S. et al., 2024 [58]	96.40%	3	670 CXR	4,05,0000	17.39s	16.56 MB
	97.89%	4	1338 CXR	4,25,0000	24.83s	17.36 MB
	98.83%	2	600 CT	3,85,0000	9.18s	15.76 MB
Soleimani-Fard, S. et al., 2024 [64]	93.42%	2	-	5,50,0000	-	600 MB
Hussein, H.I. et al., 2023 [54]	98.55	2	2762 CXR	591,903	8.86s	-
	96.83	3	3031 CXR	592,929	10.04	
Proposed CNN	99.64%	2	2544 CXR	571,015	6.12s	2.18 MB
	99.84%	2	1217 CT		12.48s	
	99.44%	3	3937 CT	571,528	17.5	
	97.13%	3	2235 CXR		7.14	
	98.27%	3	3349 CXR		10.58	
	98.76%	4	4500 CXR	572,041	15.6s	
	93.43%	4	2837 CXR		9.07	

correctly classifying the CT images. Fig. 9 and 10 shoes the training and loss curves for training and validation data and confusion matrix for test data for 2 and 3 class classification on CT dataset. The comparative analysis of proposed model and existing models for Covid-19 classification on CT images for 2 and 3 class classification task is shown in Table 16. It can also be noticed from these tables that the proposed model is performing very well over existing models for CT image classification with very few parameters comparatively. Table 16 further shows that, in comparison to the proposed 2 and 3 class classification models, the lowest parameter models for CT classification reported in the literature require 573% and 39% more parameters, respectively.

5.3. Analysis of Run time complexity and computational load

An estimation of computational complexity of the suggested models has been made in proportion to their important function in deep learning models. A direct correlation exists between the increase in network-level growth and the exponential expansion of computational complexity [65].

Utilizing the trainable parameters from the model's design is typically the first step in determining the computational complexity [66]. Thus, the computational complexity in this work was ascertained using the trainable parameters present in the architecture of the proposed model. An approximate total of 570k trainable parameters are needed for the models.

Additionally, A low computational load is maintained by the proposed model's 2.18 MB size, which is in perfect alignment with our core goal of developing a lightweight model appropriate for deployment on edge devices with constrained resources. Our model is a strong contender for deployment on devices with limited computational resources because of its remarkable accuracy as well as its efficiency regarding parameters and prediction time. The comparative analysis in terms of accuracy and computational cost is shown in Table 17.

6. Discussions

Most of the current studies reported in this work performed the classification task either on CXR or CT images. The proportion of the studies performed on the CXR images are much higher than CT images. The two most used imaging modalities for identifying pneumonia and Covid-19 are CT and CXR. It can be noticed from the table 15 that only [49,52,53,54] performed the 2 and 3 classification tasks. 3 and 4 class classification tasks on CXR images and 2 class classification tasks on CT images are performed by [58]. No study in the literature proposed the lightweight model for binary and multiclass class classification tasks on CXR and CT images both. So, in this study, performance of the proposed model is verified on both imaging modalities i.e. CXR and CT for binary as well as multiclass classification tasks.

The performance of the proposed model is verified on non-pre-processed and pre-processed datasets. Despite performing preprocessing on the CXR images, we have used the already pre-processed dataset [39]. Performance of proposed model on pre-processed dataset (X-ray dataset 2) is exceptionally remarkable with 98.76% overall accuracy for 4 class classification tasks. Our proposed model also performed well on non-pre-processed dataset (X-ray dataset 1) with 97.13% overall accuracy for 3 classes and 93.43% overall accuracy on 4 class classification tasks. Fig. 11 and 12 show the comparative analysis of F1-scores of proposed models on X-ray and CT dataset with existing studies. Results show that though the proposed model with only 570k parameters is performing well compared to existing studies on the non-pre-processed dataset, it is exceptionally performing on the pre-processed X-ray dataset and surpassing all the existing studies. The performance on the CT datasets is also remarkable specially when there are no image preprocessing techniques are applied on the CT images. Table 16 shows the comparative analysis of the proposed model performance on CT dataset with the recent studies. 99.84% and 99.44% overall accuracy for 2 and 3 class classification on CT images show the superiority of proposed our model over the existing lightweight models.

7. Strengths and Limitations

With its shorter testing time and higher computational efficiency, the proposed model reduces implementation time and requirements, making it more practical option for deployment in resource-constrained environments. Even though the proposed model produced some intriguing results, it still has several shortcomings that will be addressed in later research. Two X-ray datasets are utilized in this work. X-ray dataset 1 is applied to the model without performing any image processing on it and X-ray dataset 2 is already pre-processed dataset. Whereas, no image processing techniques are applied on CT datasets. We may investigate applying image enhancement techniques to the input images, which could improve their quality, to improve our existing method, especially for multiclass classification. Further research might be done to determine whether applying these methods could enhance the proposed model's performance.

We also understand that our proposed model is susceptible to adversarial attacks, which is important to investigate given the safety-sensitive nature of medical image identification. Adversarial attacks can cause subtle changes to input images to trick the model into making false predictions. It is crucial to comprehend and counteract these attacks to guarantee the proposed model's resilience and dependability in practical situations. We intend to investigate the problems and remedies associated with adversarial attacks in the field of medical image identification.

8. Conclusions

To effectively combat Covid-19 and making its symptoms easily identifiable, researchers are concentrating their efforts on employing DL models in this regard. However, these models are too expansive to be implemented in locations with limited resources due to their large number of parameters and high processing demands. To overcome these problems, we suggest the incredibly effective and lightweight model, to enhance the detection performance of several viral diseases of the chest, including Covid-19. Our proposed model also requires less computing power and has fewer parameters, making it more affordable. Consequently, it is more practical to diagnose individuals with infectious disorders of the chest quickly. Our proposed approach has the potential to improve the prompt and accurate identification of lung disorders, solving important issues in the field of medical imaging, by demonstrating improved performance and effective resource utilization.

Future research endeavours should be directed toward: (i) to investigate our proposed model's scalability over bigger and more varied datasets, confirming the scalability of its performance even further. (ii) various methods, including federated learning and generative adversarial networks, will also be investigated. (iii) examine whether adding more sophisticated architectural components could improve the model's ability to diagnose a wider variety of lung conditions, and (iv) to explore the

preprocessing techniques to investigate the performance.

Author Statements:

- **Ethical approval:** The conducted research is not related to either human or animal use.
- **Conflict of interest:** The authors declare that they have no known competing financial interests or personal relationships that could have appeared to influence the work reported in this paper
- **Acknowledgement:** The authors declare that they have nobody or no-company to acknowledge.
- **Funding information:** The authors declare that there is no funding to be acknowledged.
- **Data availability statement:** The data that support the findings of this study are available on request from the corresponding author. However, datasets used in this study are publicly available.

References

[1] Zhang, W. (2020). Imaging changes of severe COVID-19 pneumonia in advanced stage. *Intensive care medicine*, *46*(5), 841-843.

[2] Chen, X., Laurent, S., Onur, O. A., Kleineberg, N. N., Fink, G. R., Schweitzer, F., & Warnke, C. (2021). A systematic review of neurological symptoms and complications of COVID-19. *Journal of neurology*, *268*, 392-402.

[3] McIntosh, K. (2002). Community-acquired pneumonia in children. *New England Journal of Medicine*, *346*(6), 429-437.

[4] Goyal, S., & Singh, R. (2023). Detection and classification of lung diseases for pneumonia and Covid-19 using machine and deep learning techniques. *Journal of Ambient Intelligence and Humanized Computing*, *14*(4), 3239-3259.

[5] Gattinoni, L., Chiumello, D., Caironi, P., Busana, M., Romitti, F., Brazzi, L., & Camporota, L. (2020). COVID-19 pneumonia: different respiratory treatments for different phenotypes? *Intensive care medicine*, *46*, 1099-1102.

[6] Minaee, S., Kafieh, R., Sonka, M., Yazdani, S., & Soufi, G. J. (2020). Deep-COVID: Predicting COVID-19 from chest X-ray images using deep transfer learning. *Medical image analysis*, *65*, 101794.

[7] Haghanifar, A., Majdabadi, M. M., Choi, Y., Deivalakshmi, S., & Ko, S. (2022). Covid-cxnet: Detecting covid-19 in frontal chest x-ray images using deep learning. *Multimedia tools and applications*, *81*(21), 30615-30645.

[8] Wang, W., Xu, Y., Gao, R., Lu, R., Han, K., Wu, G., & Tan, W. (2020). Detection of SARS-CoV-2 in different types of clinical specimens. *Jama*, *323*(18), 1843-1844.

[9] Chung, M., Bernheim, A., Mei, X., Zhang, N., Huang, M., Zeng, X., ... & Shan, H. (2020). CT imaging features of 2019 novel coronavirus (2019-nCoV). *Radiology*, *295*(1), 202-207.

[10] Hertel, R., & Benlamri, R. (2022). A deep learning segmentation-classification pipeline for x-ray-based covid-19 diagnosis. *Biomedical Engineering Advances*, *3*, 100041.

[11] Thakur, S., Kasliwal, Y., Kothambawala, T., & Katarya, R. (2022). A Study on pulmonary image screening for the detection of COVID-19 using convolutional neural networks. In *Data Engineering for Smart Systems: Proceedings of SSIC 2021* (pp. 461-468). Springer Singapore.

[12] Hiremath, A., Viswanathan, V. S., Bera, K., Shiradkar, R., Yuan, L., Armitage, K., ... & Madabhushi, A. (2024). Deep Learning reveals lung shape differences on baseline chest CT between mild and severe COVID-19: A multi-site retrospective study. *Computers in Biology and Medicine*, 108643.

[13] Ieracitano, C., Mammone, N., Versaci, M., Varone, G., Ali, A. R., Armentano, A., ... & Morabito, F. C. (2022). A fuzzy-enhanced deep learning approach for early detection of Covid-19 pneumonia from portable chest X-ray images. *Neurocomputing*, *481*, 202-215.

[14] Subramanian, N., Elharrouss, O., Al-Maadeed, S., & Chowdhury, M. (2022). A review of deep learning-based detection methods for COVID-19. *Computers in Biology and Medicine*, *143*, 105233.

[15] Agnihotri, A., & Kohli, N. (2023). Challenges, opportunities, and advances related to COVID-19 classification based on deep learning. *Data Science and Management*, *6*(2), 98-109.

[16] Akhtar, F., Heyat, M. B. B., Li, J. P., Patel, P. K., & Guragai, B. (2020, December). Role of machine learning in human stress: a review. In *2020 17th International Computer Conference on Wavelet Active Media Technology and Information Processing (ICCWAMTIP)* (pp. 170-174). IEEE.

[17] Ukwuoma, C. C., Zhiguang, Q., Bin Heyat, M. B., Ali, L., Almaspoor, Z., & Monday, H. N. (2022). Recent advancements in fruit detection and classification using deep learning techniques. *Mathematical Problems in Engineering*, *2022*(1), 9210947.

[18] Guragai, B., AlShorman, O., Masadeh, M., & Heyat, M. B. B. (2020, December). A survey on deep learning classification algorithms for motor imagery. In *2020 32nd international conference on microelectronics (ICM)* (pp. 1-4). IEEE.

[19] AlShorman, O., Masadeh, M., Heyat, M. B. B., Akhtar, F., Almahasneh, H., Ashraf, G. M., &

Alexiou, A. (2022). Frontal lobe real-time EEG analysis using machine learning techniques for mental stress detection. *Journal of integrative neuroscience*, *21*(1), 20.

[20] Bin Heyat, M. B., Akhtar, F., Abbas, S. J., Al-Sarem, M., Alqarafi, A., Stalin, A., ... & Wu, K. (2022). Wearable flexible electronics based cardiac electrode for researcher mental stress detection system using machine learning models on single lead electrocardiogram signal. *Biosensors*, *12*(6), 427.

[21] Teelhawod, B. N., Akhtar, F., Heyat, M. B. B., Tripathi, P., Mehrotra, R., Asfaw, A. B., ... & Masadeh, M. (2021, October). Machine learning in E-health: a comprehensive survey of anxiety. In *2021 International Conference on Data Analytics for Business and Industry (ICDABI)* (pp. 167-172). IEEE.

[22] Heyat, M. B., Akhtar, F., Khan, M. H., Ullah, N., Gul, I., Khan, H., & Lai, D. (2021). Detection, treatment planning, and genetic predisposition of bruxism: a systematic mapping process and network visualization technique. *CNS & Neurological Disorders-Drug Targets (Formerly Current Drug Targets-CNS & Neurological Disorders)*, *20*(8), 755-775.

[23] Bin Heyat, M. B., Akhtar, F., Khan, A., Noor, A., Benjdira, B., Qamar, Y., ... & Lai, D. (2020). A novel hybrid machine learning classification for the detection of bruxism patients using physiological signals. *Applied Sciences*, *10*(21), 7410.

[24] Aggarwal, P., Mishra, N. K., Fatimah, B., Singh, P., Gupta, A., & Joshi, S. D. (2022). COVID-19 image classification using deep learning: Advances, challenges and opportunities. *Computers in Biology and Medicine*, *144*, 105350.

[25] LeCun, Y., Bengio, Y., & Hinton, G. (2015). Deep learning. *nature*, *521*(7553), 436-444.

[26] Li, Y., Daho, M. E. H., Conze, P. H., Zeghlache, R., Le Boité, H., Tadayoni, R., ... & Quellec, G. (2024). A review of deep learning-based information fusion techniques for multimodal medical image classification. *Computers in Biology and Medicine*, 108635.

[27] Hassantabar, S., Wang, Z., & Jha, N. K. (2021). SCANN: Synthesis of compact and accurate neural networks. *IEEE Transactions on Computer-Aided Design of Integrated Circuits and Systems*, *41*(9), 3012-3025.

[28] Hassantabar, S., Dai, X., & Jha, N. K. (2019). STEERAGE: Synthesis of neural networks using architecture search and grow-and-prune methods. *arXiv preprint arXiv:1912.05831*.

[29] Bullock, J., Luccioni, A., Pham, K. H., Lam, C. S. N., & Luengo-Oroz, M. (2020). Mapping the landscape of artificial intelligence applications against COVID-19. *Journal of Artificial Intelligence Research*, *69*, 807-845.

[30] Al-Antari, M. A., Al-Masni, M. A., Choi, M. T., Han, S. M., & Kim, T. S. (2018). A fully integrated computer-aided diagnosis system for digital X-ray mammograms via deep learning detection, segmentation, and classification. *International journal of medical informatics*, *117*, 44-54.

[31] Al-Masni, M. A., Al-Antari, M. A., Park, J. M., Gi, G., Kim, T. Y., Rivera, P., ... & Kim, T. S. (2018). Simultaneous detection and classification of breast masses in digital mammograms via a deep learning YOLO-based CAD system. *Computer methods and programs in biomedicine*, *157*, 85-94.

[32] Gour, M., & Jain, S. (2022). Uncertainty-aware convolutional neural network for COVID-19 X-ray images classification. *Computers in biology and medicine*, *140*, 105047.

[33] Zhu, X., Lyu, S., Wang, X., & Zhao, Q. (2021). TPH-YOLOv5: Improved YOLOv5 based on transformer prediction head for object detection on drone-captured scenarios. In *Proceedings of the IEEE/CVF international conference on computer vision* (pp. 2778-2788).

[34] Vaswani, A. (2017). Attention is all you need. *arXiv preprint arXiv:1706.03762*.

[35] Iandola, F. N., Han, S., Moskewicz, M. W., Ashraf, K., Dally, W. J., & Keutzer, K. (2016). SqueezeNet: AlexNet-level accuracy with 50x fewer parameters and< 0.5 MB model size. *arXiv preprint arXiv:1602.07360*.

[36] https://www.kaggle.com/datasets/tawsifurrahman/covid19-radiography-database.

[37] https://www.kaggle.com/datasets/anasmohammedtahir/covidqu.

[38] https://www.kaggle.com/datasets/paultimothymooney/chest-xray-pneumonia.

[39] Roy, S., Tyagi, M., Bansal, V., & Jain, V. (2022). Svd-clahe boosting and balanced loss function for covid-19 detection from an imbalanced chest x-ray dataset. *Computers in Biology and Medicine*, *150*, 106092.

[40] Ning, W., Lei, S., Yang, J., Cao, Y., Jiang, P., Yang, Q., ... & Wang, Z. (2020). iCTCF: an integrative resource of chest computed tomography images and clinical features of patients with COVID-19 pneumonia.

[41] Islam, M. N., Hasan, M., Masum, A. K. M., Uddin, M. Z., & Alam, M. G. R. (2021, December). Demystify the black-box of deep learning models for covid-19 detection from chest ct radiographs. In *2021 24th International Conference on Computer and Information Technology (ICCIT)* (pp. 1-6). IEEE.

[42] Özyurt, F., Sert, E., & Avcı, D. (2020). An expert system for brain tumor detection: Fuzzy C-means with super resolution and convolutional neural network with extreme learning machine. *Medical hypotheses*, *134*, 109433.

[43] Jadhav, P., Rajguru, G., Datta, D., & Mukhopadhyay, S. (2020). Automatic sleep stage classification using time–frequency images of CWT and transfer learning using convolution neural network. *Biocybernetics and Biomedical Engineering*, *40*(1), 494-504.

[44] Hu, J., Shen, L., & Sun, G. (2018). Squeeze-and-excitation networks. In *Proceedings of the IEEE conference on computer vision and pattern recognition* (pp. 7132-7141).

[45] Shu, X., Chang, F., Zhang, X., Shao, C., & Yang, X. (2022). ECAU-Net: Efficient channel attention U-Net for fetal ultrasound cerebellum segmentation. *Biomedical Signal Processing and Control*, *75*, 103528.

[46] Wang, Q., Wu, B., Zhu, P., Li, P., Zuo, W., & Hu, Q. (2020). ECA-Net: Efficient channel attention for deep convolutional neural networks. In *Proceedings of the IEEE/CVF conference on computer vision and pattern recognition* (pp. 11534-11542).

[47] Shi, Y., Wang, Z., Du, X., Ling, G., Jia, W., & Lu, Y. (2022). Research on the membrane fouling diagnosis of MBR membrane module based on ECA-CNN. *Journal of Environmental Chemical Engineering*, *10*(3), 107649.

[48] Lin, X., Huang, Q., Huang, W., Tan, X., Fang, M., & Ma, L. (2021). Single image deraining via detail-guided efficient channel attention network. *Computers & Graphics*, *97*, 117-125.

[49] George, G. S., Mishra, P. R., Sinha, P., & Prusty, M. R. (2023). COVID-19 detection on chest X-ray images using Homomorphic Transformation and VGG inspired deep convolutional neural network. *Biocybernetics and Biomedical Engineering*, *43*(1), 1-16.

[50] Jyoti, K., Sushma, S., Yadav, S., Kumar, P., Pachori, R. B., & Mukherjee, S. (2023). Automatic diagnosis of COVID-19 with MCA-inspired TQWT-based classification of chest X-ray images. *Computers in Biology and Medicine*, *152*, 106331.

[51] Malik, D., Anjum, & Katarya, R. (2022). Comparative analysis by transfer learning of pre-trained models for detection of covid-19 using chest x-ray images. In *Proceedings of the International Conference on Paradigms of Communication, Computing and Data Sciences: PCCDS 2021* (pp. 549-557). Springer Singapore.

[52] Ukwandu, O., Hindy, H., & Ukwandu, E. (2022). An evaluation of lightweight deep learning techniques in medical imaging for high precision COVID-19 diagnostics. *Healthcare Analytics*, *2*, 100096.

[53] Nayak, S. R., Nayak, D. R., Sinha, U., Arora, V., & Pachori, R. B. (2022). An efficient deep learning method for detection of COVID-19 infection using chest X-ray images. *Diagnostics*, *13*(1), 131.

[54] Hussein, H. I., Mohammed, A. O., Hassan, M. M., & Mstafa, R. J. (2023). Lightweight deep CNN-based models for early detection of COVID-19 patients from chest X-ray images. *Expert Systems with Applications*, *223*, 119900.

[55] Pradeep Dalvi, P., Reddy Edla, D., Purushothama, B. R., & Dharavath, R. (2024). COVID-19 detection from Chest X-ray images using a novel lightweight hybrid CNN architecture. *Multimedia Tools and Applications*, 1-23.

[56] Ainapure, B. S., Appasani, B., Schiopu, A. G., Oproescu, M., & Bizon, N. (2024). A Lightweight Deep Learning Model and Web Interface for COVID-19 Detection Using Chest X-Rays. *Traitement du Signal*, *41*(1).

[57] Wang, S., Ren, J., & Guo, X. (2024). A high-accuracy lightweight network model for X-ray image diagnosis: A case study of COVID detection. *PloS one*, *19*(6), e0303049.

[58] Asif, S., Zhao, M., Tang, F., & Zhu, Y. (2024). LWSE: a lightweight stacked ensemble model for accurate detection of multiple chest infectious diseases including COVID-19. *Multimedia Tools and Applications*, *83*(8), 23967-24003.

[59] Huang, M. L., & Liao, Y. C. (2022). A lightweight CNN-based network on COVID-19 detection using X-ray and CT images. *Computers in Biology and Medicine*, *146*, 105604.

[60] Ahamed, K. U., Islam, M., Uddin, A., Akhter, A., Paul, B. K., Yousuf, M. A., ... & Moni, M. A. (2021). A deep learning approach using effective preprocessing techniques to detect COVID-19 from chest CT-scan and X-ray images. *Computers in biology and medicine*, *139*, 105014.

[61] Sanida, T., Sideris, A., Tsiktsiris, D., & Dasygenis, M. (2022). Lightweight neural network for COVID-19 detection from chest X-ray images implemented on an embedded system. *Technologies*, *10*(2), 37.

[62] Asham, M. A., Al-Shargabi, A. A., Al-Sabri, R., & Meftah, I. (2024). A lightweight deep learning model with knowledge distillation for pulmonary diseases detection in chest X-rays. *Multimedia Tools and Applications*, 1-29.

[63] Asif, S., Ain, Q. U., Al-Sabri, R., & Abdullah, M. (2024). LitefusionNet: Boosting the Performance for Medical Image Classification with an Intelligent and Lightweight Feature Fusion Network. *Journal of Computational Science*, 102324.

[64] Soleimani-Fard, S., & Ko, S. B. (2024). Res-MGCA-SE: a lightweight convolutional neural network based on vision transformer for medical image classification. *Neural Computing and Applications*, 1-14.

[65] Fang, L., & Wang, X. (2022). COVID-RDNet: A novel coronavirus pneumonia classification model using the mixed dataset by CT and X-rays images. *biocybernetics and biomedical engineering*, *42*(3), 977-994.

[66] Sarv Ahrabi, S., Scarpiniti, M., Baccarelli, E., & Momenzadeh, A. (2021). An accuracy vs. complexity comparison of deep learning

architectures for the detection of COVID-19 disease. *Computation*, *9*(1), 3.

[67] Yasar, H. and Ceylan, M., 2024. Deep Learning–Based Approaches to Improve Classification Parameters for Diagnosing COVID-19 from CT Images. *Cognitive Computation*, *16*(4), pp.1806-1833.

[68] Hassan, E., Shams, M.Y., Hikal, N.A. and Elmougy, S., 2024. Detecting COVID-19 in chest CT images based on several pre-trained models. *Multimedia Tools and Applications*, pp.1-21.

[69] Zhang, H., Lv, Z., Liu, S., Sang, Z. and Zhang, Z., 2024. Cn2a-capsnet: a capsule network and CNN-attention based method for COVID-19 chest X-ray image diagnosis. *Discover Applied Sciences*, *6*(4), p.190.